Egyptian Journal of Chemistry

http://ejchem.journals.ekb.eg/

Comparative Study of Textural Properties for Various Silica by Nitrogen Adsorption-desorption Technique

Badoor M. Kurji, [a] Ammar S. Abbas [b]*

[a] *Department of Chemical and Petrochemical Engineering, College of Engineering, University of Anbar, Anbar, Iraq*
[b] *Chemical Engineering Department, College of Engineering, University of Baghdad, Baghdad, Iraq*

Abstract

This work studied the textual properties of the MCM-48 and rice husk ash using nitrogen adsorption-desorption at constant low temperatures. According to the International Union of Pure and Applied Chemistry, the adsorption-desorption isotherm proved that the studied materials have a mesoporous structure with type IV. The obtained results of Langmuir, Freundlich, and Brunauer–Emmett–Teller isotherm models showed that the nitrogen adsorption followed Brunauer–Emmett–Teller isotherm. The found adsorption capacity and surface area values for MCM-48 were higher than those values for rice husk ash. Based on the Kelvin equation, Barrett, Joyner, and Halenda model was used to determine pore size distribution, pore diameter, and average pore volume for the adsorbents. The pore size distribution for MCM-48 was narrower than rice husk ash, pore diameter for MCM-48 was less than rice husk ash, and average pore volume for MCM-48 was higher than the value of average pore volume for rice hush ash. The comparison study results between the properties and those previously published for mesoporous materials indicated a convergence in the surface area of MCM-48 and pore volume. Moreover, the results of the comparison between the properties of rice husk ash showed that the surface area and pore volume were equal or less than those obtained before.

Keywords: MCM-48; rice husk ash; mesoporous; adsorption isotherms; surface area; pore size distribution

1. Introduction

Silica is an inorganic chemical compound plentifully available in the earth incrustation [1]. Still, despite being abundant, silica is generally made by way of synthesis for use mainly in the preparation of different types of adsorbents [2-4] and catalysts [5-15] used in chemical applications. Silica generally exists as alkoxysilane compounds, which can harm health. Therefore, other safer, cheaper, and more environmentally friendly sources of silica are constantly being sought [1]. Agricultural waste is one of the most critical renewable silica sources, which are low-cost sources of natural silica like rice husk, rice straw, corn cobs, and bagasse [16, 17]. Rice husk ash (RHA) is rich in amorphous silica (SiO_2) and other metallic contaminants, which can be obtained after burning rice husk [4,18] and used to make silicon-based products [19]. MCM-48 is a nanostructured mesoporous material that belongs to the M41S family (mesoporous silica). MCM-48 is getting more attention because of its large surface area (SA), strong

acidity, and excellent hydrothermal stability [20]. The huge SA of the MCM-48 and organized pore structure and narrow pore size distribution (PSD) belong to its three-dimensional structure [21, 22]. Commonly, mesoporous materials with pore diameters of 2–50 nm act as promising catalysts for various reactions and successful adsorbents for adsorption and separation [20].

Gas adsorption-desorption is the most technique for the characterization of porous solids. The adsorption-desorption process is considered standard for determining solid materials SA and PSD [23, 24]. Adsorption is the phenomenon defined by the adhesion of a chemical species (adsorbate) onto or near the surfaces and pores of the solid (adsorbent). [25]. The adsorption process may be physical or chemical adsorption; the physical adsorption is related to Van der Wales forces generated by the film of adsorbate. In comparison, chemical reactions between adsorbate and adsorbent are cause chemical adsorption [26].

_____

The amount of gas adsorbed onto a solid surface or its pore space is proportional to the solid SA, temperature, the partial equilibrium pressure of the gas, and the nature of the solid and gas. The adsorption isotherm is the relationship between the amount of gas adsorbed per unit mass of material and pressure at a specific temperature [25]. Adsorption isotherms are classified into six categories by the International Union of Pure and Applied Chemistry (IUPAC) based on the isotherm shape of relative pressure and amount of gas adsorbed onto a solid surface [27]. Different gases can be used for adsorption-desorption, such as carbon dioxide, argon, and nitrogen (N_2). Among these various gases and vapors, which are readily available and could be used as adsorbate, N_2 (measured at 77 K) has remained universally well-known and considered friendly commercial equipment [28].

In general, different adsorption models that are used to describe adsorption isotherms experimental data [28].

This work aims to comparatively study the nature of the adsorption process and textural properties of selected silica (MCM-48 and RHA) by analyses of N_2 adsorption-desorption at 77 K data, which describe using different isotherm models. The SA of the samples was measured by the Brunauer–Emmett–Teller (BET) method. PSD was calculated by the Barrett–Joyner–Halenda (BJH) method, and the founded results were compared with the previous studies.

2. Experimental and theoretical work

2.1. Adsorption-desorption tests

N_2 adsorption-desorption over samples of MCM-48 (0.0485 g) and RHA (0.2144 g) were measured at 77 K using the TriStar I 2.03 (micromeritics) apparatus. All experiments were conducted at the Sharif University of Technology in Tehran, Iran. Each measurement was repeated twice, and the average values of the obtained readings were recorded and used later in the analyses of the isotherm models and determination of SA and PSD.

2.2. Langmuir isotherm model

Langmuir described the isotherm model of gas adsorption on a solid phase in 1916 [31]. This empirical model assumes that the thickness of the adsorbed layer is monolayer adsorption and that the adsorption process occurs at similar and equivalent

definite localized sites [30]. A convenient form of the Langmuir shown in Eq. (1).

$$\frac{P}{Q} = \frac{P}{Q_m} + \frac{1}{Q_m K_L} \qquad (1)$$

Where; where P (mmHg) is the equilibrium pressure, and Q (cm^3/ g (STP)) volume of nitrogen adsorbed at a given pressure and constant temperature, Q_m (cm^3/ g (STP)) maximum volume of nitrogen adsorbed to form a complete monolayer on the solid surface, respectively. The term K_L (1/mmHg) is a Langmuir constant which indicates the extent of interaction between gas and solid surface, which can be correlated with the variation of the suitable area and porosity of the adsorbent, which implies that large SA and pore volume (V_P) will result in higher adsorption capacity [32, 33]. A plot of P/Q versus P should give a straight. The slope and intercept of the straight line can find the monolayer maximum adsorption capacity and Langmuir constant.

2.3. Freundlich isotherm model

Freundlich published a model in 1906 [34] that describes the relationship between pressure and the amount of gas adsorbed by a unit mass of solid adsorbent at a constant temperature [35]. The Freundlich isotherm equation expressed as Eq. (2).

$$LogQ = LogK_f + \frac{1}{n}LogP \qquad (2)$$

Where, Q (cm^3/ g (STP)) volume of nitrogen adsorbed at a given pressure and constant temperature, K_f is Freundlich constant and n is the heterogeneity factor [36].

2.4. BET isotherm model

The SA is approximated using the BET equation from a particular region of a gas adsorption isotherm where monolayers of gas are thought to take place, after the publication of the BET theory [26]. The adsorption of a gas on the surface of a material is the essential ingredient of the BET theory. For this reason, the BET equation, which was created to explain the multilayer adsorption of gas molecules on a solid surface, is often utilized. The BET analysis is based on the adsorption isotherms of nonreactive gas molecules such as nitrogen or argon at a pressure range encompassing the monolayer coverage of molecules [37]. The BET isotherm is a theoretical equation that

is used to calculate the SA of gas-solid equilibrium systems Eq. (3) [30].

$$\frac{\left(\frac{P}{P_o}\right)}{Q\left[1-\left(\frac{P}{P_o}\right)\right]} = \frac{C-1}{Q_m C}\left(\frac{P}{P_o}\right) + \frac{1}{Q_m C} \qquad (3)$$

Where; Q (cm^3/ g (STP)) volume of nitrogen adsorbed at a given pressure and constant temperature, Q_m (cm^3/g (STP)) maximum volume of nitrogen adsorbed to form a complete monolayer on the solid surface, and C is constant related to the difference between the heat of adsorption in the first layer and the heat of liquefaction of the vapor [25]. Application of the BET equation to the nitrogen adsorption data obtained in the present study was only possible within a narrow range of relative pressures (0.05-0.3) [38]. A plot of $\left(\frac{P}{P_o}\right)\Big/\left(Q\left(1-\left(\frac{P}{P_o}\right)\right)\right)$ versus $\left(\frac{P}{P_o}\right)$ should yield a straight line with a positive slope, then Q_m and C can be determined from intercept and slop [39].

2.5. Determination of SA

SA of samples determined by using Eq. (4) [40].

$$SA = \frac{Q_m L_{av} A_m}{M} \qquad (4)$$

Where; L_{av} is Avogadro number, A_m is the cross-sectional area of the adsorbate and equals 0.162 nm^2 for a N_2 molecule, M is the molar volume for nitrogen which equals 22.414 L/mole.

2.6. BJH pore diameter and volume

The PSD, Barrett–Joyner–Halenda pore diameter (d_{BJH}) and V_P for the adsorbent, can be calculated using N_2 adsorption-desorption isotherm data at 77 K. This model was developed by Barrett–Joyner–Halenda in 1951 [41] by assuming the pore shapes are cylindrical with finite length and open ends. Also, this model assumed pore radius was the sum of Kelvin radius and thickness of the adsorbed film as seen in Eq. (5) [42-44].

$$\ln\left(\frac{P}{P_o}\right) = -\frac{C\gamma v \cos\theta}{RT(r-t)} \qquad (5)$$
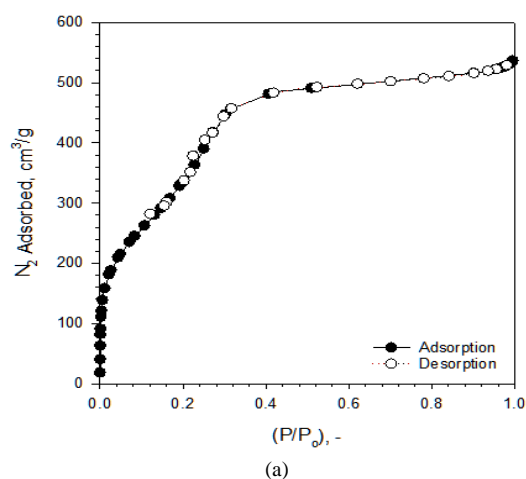
Where P is the critical condensation pressure, γ the liquid surface tension, v the molar volume of the condensed adsorptive, θ the contact angle between the solid and condensed phase, r the radius of curvature of the liquid, P/P_o relative pressure, R gas constant, and T temperature. C constant depends on the curvature equal to 2 in case of cylindrical shaped and t is the thickness of adsorbed layer remaining on the pare walls, which can be calculated by the Halsey equation (Eq. (6)) [44].

$$t = 3.54\left(\frac{-5}{\ln\left(\frac{P}{P_o}\right)}\right)^{0.333} \qquad (6)$$

3. Results and discussion

The N_2 adsorption-desorption data was used to identify the isotherm type and hence the nature of the adsorption process for the selected material. The N_2 adsorption-desorption isotherms over the surface of the MCM-48 and RHA were shown in Fig.1. As shown in Fig.1, MCM-48 was adsorbed more N_2 quantity than RHA. Fig.1 (a) showed that the amount of N_2 absorbed by MCM-48 reached a value of 536 cm^3/g, while the RHA absorbed only 165 cm^3/g as shown in Fig.1 (b). According to the adsorption-desorption data shapes, the MCM-48 and RHA could be classified as types IV (b) and IV (a), depending on the IUPAC classification, which is referred to as mesoporous materials [45].
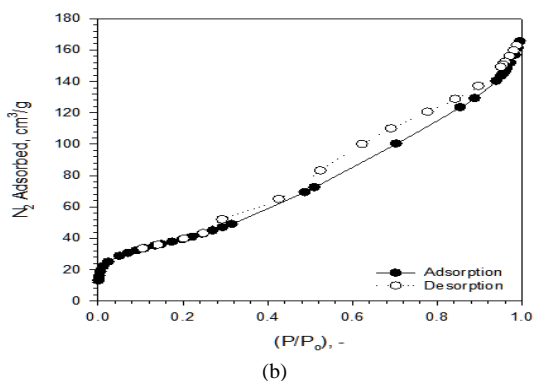

(a)

(b)

Figure 1. N_2 adsorption-desorption isotherm (a) MCM-48 (b) RHA.

The isotherm curve for MCM-48 adsorbents having smaller mesoporous showed a completely reversible adsorption behaviour. No significant hysteresis was found between the adsorption and desorption isotherms, leading to a type IV (b) isotherm [46]. In contrast, the RHA curve shows a hysteresis when the pore diameter is larger than approximately 4 nm for nitrogen adsorption at 77 K [47]. The desorption branch for RHA does not follow the adsorption branch but gives a distinct hysteresis loop, where the amount adsorbed is more significant along the desorption branch than the adsorption branch; the hysteresis loop can be classified as type H3 according to the IUPAC [47].

Langmuir, Freundlich, and BET isotherm models were used to describe the experimental data of N_2 adsorption on the surface of MCM-48 and RHA to find the best fitting isotherm model and determine the capacity of the adsorbent. The isotherm models for MCM-48 and RHA were shown in Fig.2 to 4. Fig.2 shows the Langmuir isotherm model (Eq.1) for MCM-48 and RHA. This isotherm described the N_2 adsorption data better for MCM-48 (Fig.2, a) with correlation coefficient (R^2) equal to 0.9883, while this isotherm model did not fit the adsorption data for RHA (Fig.2, b).

The Freundlich isotherm model (Eq. 2) shown in Fig.3 described both the adsorption data considerably with R^2 equal 0.9768 for MCM-48 and 0.8388 for RHA. Fig.4 showed the BET isotherm model (Eq. 3), which described the N_2 adsorption data perfectly for both mesoporous silica with R^2 equal to 0.9975 and 0.9992 for MCM-48 and RHA, respectively. The isotherm models constants for both MCM-48 and RHA were reported in Table 1. The value of adsorption capacity, determined by the BET isotherm model, for MCM-48 is equal to 312.5 cm^3/g and 33.89 cm^3/g for RHA. The SA of MCM-48 and RHA were estimated by the BET model (Eq. 4), and were 1360.14 m^2/g for MCM-48

and 147.51 m^2/g for RHA. The SA of MCM-48 was higher than the SA of RHA because MCM-48 has a cubic structure system, which is indexed in the space group Ia3d [48].
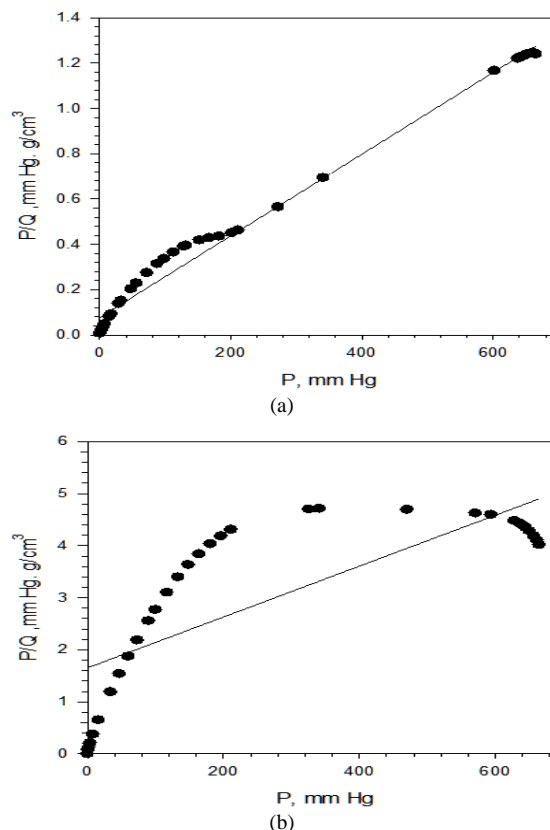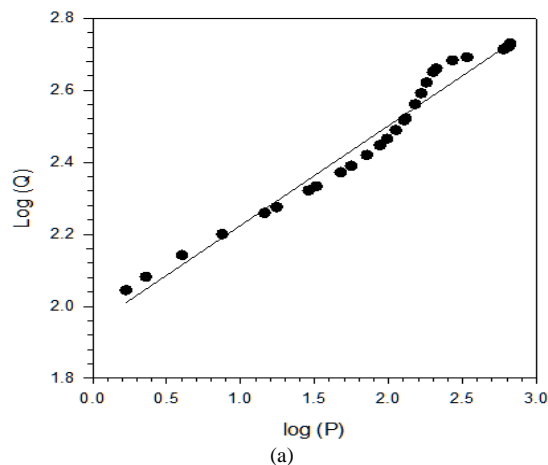

(a)

(b)

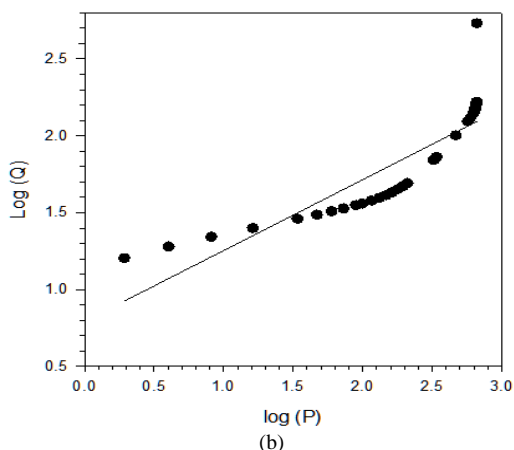Figure 2. N_2 adsorption isotherm by Langmuir model (a) MCM-48 (b) RHA.

(a)

(b)

Figure 3. N$_2$ adsorption isotherm by Freundlich model (a) MCM-48 (b) RHA.
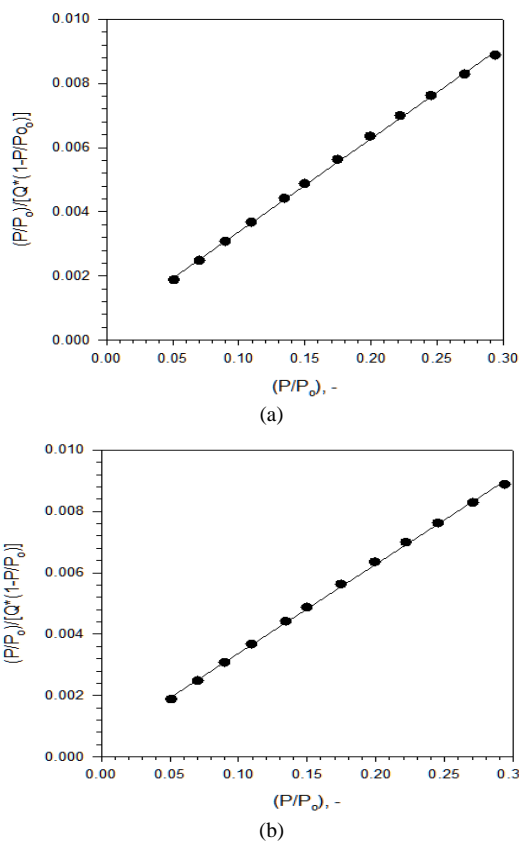

(a)

(b)

Figure 4. N$_2$ adsorption isotherm by Brunauer–Emmett–Teller (a) MCM-48 (b) RHA.

Table 1:The constants and R^2 for the isotherm models

Isotherm model		MCM-48	RHA
Langmuir	Q_m (cm^3/g)	555.5	212.76
	K_L(1/mmHg)	0.023	2.647
	R^2	0.9883	0.6017
Freundlich	K_f	88.756	6.840
	n	3.601	2.311
	R^2	0.9768	0.8388
BET	Q_m(cm^3/g)	312.5	33.89
	C	32	59
	R^2	0.9975	0.9992

BJH model and N$_2$ adsorption data at 77 K have been utilized to find the PSD (Fig.5) for the studied mesoporous adsorbents (MCM-48 and RHA). PSD for MCM-48 (Fig.5, a) was narrower than RHA (Fig.5, b). The two materials PSD peaks (the mode pore size diameter) existed at 2.38 nm for MCM-48 and 3.62 nm for RHA. At the same time, the total pore volumes were 1.030 cm^3/g for MCM-48 and 0.292 cm^3/g for RHA.
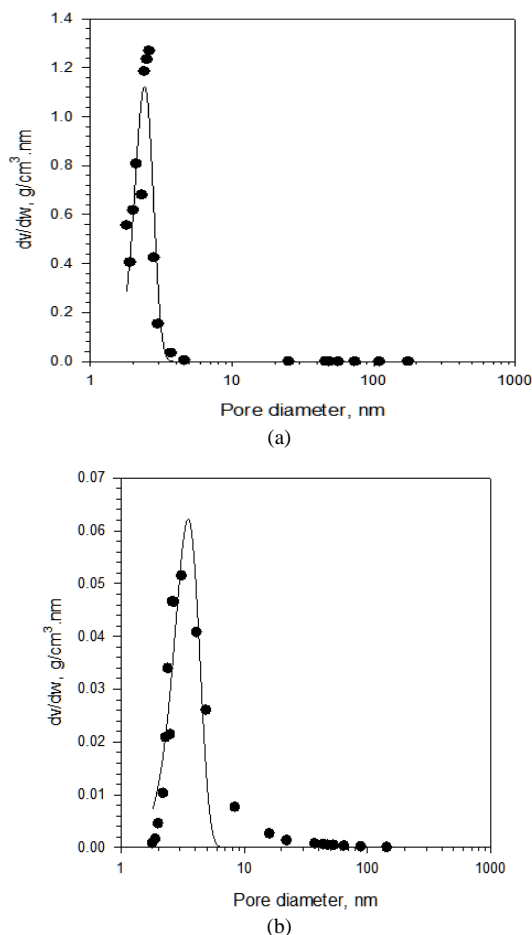

(a)

(b)

Figure 5. BJH particle size distribution for (a) MCM-48 (b) RHA.

A comparison of textural properties was made and summarized in Table 2 between the currently obtained results for MCM-48 and RHA and different properties for mesoporous silica having the same porous structure reported in previous works [4,14,20,22, 49-51]. The SA of the current MCM-48 was 1360.14 m^2/g which was in the same magnitude as the reported values for MCM-48 [14,20,22], and MCM-41 [49]. However, the value SA of the current MCM-48 was higher than the reported SA of the previously prepared MCM-48 [14], mesoporous silica-alumina [49], and Santa Barbara Amorphous-15 (SBA-15) [50].

However, the SA of the current RHA was 147.51 m²/g which was approximately equal to the SA of the previously prepared RHA [4] and lower than the reported SA of RHA [51]. The Vp value of the current MCM-48 was 1.030 cm³/g, which was higher than the reported values for MCM-48 [14,20,22], MCM-41 [49], SBA-15 [50], and mesoporous silica-alumina [49]. Although, the Vp for the current RHA (0.292 cm³/g) was in the same range as the previously prepared RHA [4] and lower than the reported RHA obtained from the different origin [51].

Table 2

Textural properties for different silica obtained from N_2 adsorption at 77 K

Silica type	BET SA, m²/g	V_P, cm³/g	d_{BJH}, nm	Reference
MCM-48	1360.14	1.030	2.38	Current study
MCM-48	1028.95	0.69	2.68	[20]
MCM-48	1520	0.74	--	[22]
MCM-48	669	0.33	--	[14]
MCM-41	972	0.65	2.6	[49]
Santa Barbara Amorphous-15 (SBA-15)	771	1.00	--	[50]
mesoporous silica-alumina	830	0.46	3.8	[49]
RHA	147.51	0.292	3.62	Current study
RHA	148.53	0.254	--	[4]
RHA	589	0.75	5.1	[51]

SA: BET surface area, V_P: pore volume, d_{BJH}: pore diameter by BJH

4. Conclusions

According to the IUPAC, the adsorption-desorption isotherm proved that the MCM-48 and RHA have a mesoporous structure with type IV. MCM-48 type IV(b) with no significant loop, while RHA had type IV(a) with H3 hysteresis loop. Langmuir and Freundlich isotherm models did not fit experimental data for MCM-48 and RHA. In contrast, the BET isotherm model was the best isotherm model that described the experimental data for two selected materials. The adsorption capacities determined by the BET isotherm model were 312.5 cm³/g for MCM-48 and 33.89 cm³/g for RHA, and the SA for MCM-48 and RHA were 1360.14 m²/g and 147.51 m²/g, respectively. By BJH model, PSD for MCM-48 was narrower than RHA, d_{BJH} for MCM-48 was 2.38 nm and 3.62 nm for RHA, and V_P was 1.030 cm³/g for MCM-48 and 0.292 cm³/g for RHA. The comparison study results between the properties and those previously published for mesoporous materials indicated a convergence in the SA of MCM-48 and V_p.

Moreover, the comparison results between the SA and V_P of RHA were equal and less than those values for RHA obtained before.

5. References

[1] N. Permatasari, T. N. Sucahya, and A. B. D. Nandiyanto, Review: Agricultural wastes as a source of silica material. *Indonesian Journal of Science and Technology*, 1(1), 82–106(2016), doi: 10.17509/ijost.v1i1.8619.

[2] A. S. Abbas and S. A. Hussien, Equilibrium Kinetic and Thermodynamic Study of Aniline Adsorption over Prepared ZSM-5 Zeolite. *Iraqi Journal of Chemical and Petroleum Engineering*, 18 (1), 47–56 (2017), doi: 10.31699/IJCPE.

[3] S. K. A. Barno, H. J. Mohamed, S. M. Saeed, and M. J. Al-, Prepared 13X Zeolite as a Promising Adsorbent for the Removal of Brilliant Blue Dye from Wastewater. *Iraqi Journal of Chemical and Petroleum Engineering*, 2 (2), 1–6 (2021).

[4] H. Abbas and A. S. Abbas, Adsorption of Flagyl on Prepared Ash from Rice Husk. *Iraqi Journal of Chemical and Petroleum Engineering*, 22 (4), 11–17 (2021), doi: 10.31699/IJCPE.2021.4.2.

[5] A. S. Abbas and R. N. Abbas, Kinetic Study and Simulation of Oleic Acid Esterification over Prepared NaY Zeolite Catalyst. *Iraqi Journal of Chemical and Petroleum Engineering*, 14 (4), 35–43 (2013).

[6] A. S. Abbas and R. N. Abbas, Preparation and Characterization of Nay Zeolite for Biodiesel Production. *Iraqi Journal of Chemical and Petroleum Engineering*, 16 (2), 19–29, (2015).

[7] B. A. Alshahidy and A. S. Abbas, Comparative Study on the Catalytic Performance of a 13X Zeolite and its Dealuminated Derivative for Biodiesel Production. *Bulletin of Chemical Reaction Engineering & Catalysis Journal*, 16 (4), 763–772 (2021), doi: 10.9767/bcrec.16.4.11436.763-772.

[8] A. S. Abbas, T. M. Albayati, Z. T. Alismaeel, and A. M. Doyle, Kinetics and Mass Transfer Study of Oleic Acid Esterification over Prepared Nanoporous HY zeolite. *Iraqi Journal of Chemical and Petroleum Engineering*, 17 (1), 47–60, (2016).

[9] Ammar S. Abbas; and M. G. Saber, Thermal and Catalytic Degradation Kinetics of High-Density Polyethylene over NaX Nano- Zeolite. *Iraqi Journal of Chemical and Petroleum Engineering*, 17 (3), 33–43(2016).

[10] A. M. Doyle, T. M. Albayati, A. S. Abbas, and Z. T. Alismaeel, Biodiesel production by esterification of oleic acid over zeolite Y prepared from kaolin. *Renew. Energy*, 97, -19–23 (2016), doi: 10.1016/j.renene.2016.05.067.

[11] A. M. Doyle, Z. T. Alismaeel, T. M. Albayati, and A. S. Abbas, High purity FAU-type zeolite catalysts from shale rock for biodiesel production. *Fuel Journal*, 199, 394–402 (2017), doi: 10.1016/j.fuel.2017.02.098.

[12] Z. T. Alismaeel, A. S. Abbas, T. M. Albayati, and A. M. Doyle, Biodiesel from batch and continuous oleic acid esterification using zeolite catalysts. *Fuel Journal*, 234, 170–176 (2018), doi: 10.1016/j.fuel.2018.07.025.

[13] A. S. Abbas, M. Y. Hussein, and H. J. Mohammed, Preparation of solid catalyst suitable for biodiesel production. *Plant Archives Journal*, 19 (2), 3853–3861 (2019).

[14] A. H. Alfattal and A. S. Abbas, Synthesized 2nd Generation Zeolite as an Acid-Catalyst for Esterification Reaction. *Iraqi Journal of Chemical and Petroleum Engineering*, 20 (3), 67–73, (2019), doi: 10.31699/IJCPE.2019.3.9.

[15] B. A. Alshahidy and A. S. Abbas, Preparation and Modification of 13X Zeolite as a Heterogeneous Catalyst for Esterification of Oleic Acid. *AIP Conference Proceedings*, 2213 (1), (2020), doi: 10.1063/5.0000171.

[16] S. K. S. Hossain, L. Mathur, and P. K. Roy, Rice husk/rice husk ash as an alternative source of silica in ceramics: A review. *Asian Ceramic Societies Journal*, 6 (4), 299–313, (2018), doi: 10.1080/21870764.2018.1539210.

[17] J. Chun and J. H. Lee, Recent progress on the development of engineered silica particles derived from rice husk. *Sustainability Journal*, 12 (24), 1–19, (2020), doi: 10.3390/su122410683.

[18] C. Siriluk and S. Yuttapong, Structure of Mesoporous MCM-41 Prepared from Rice Husk Ash. *The 8th Asian Symposium on Visualization*, May 23-27 (2005).

[19] A. S. Costa and C. M. Paranhos, Systematic evaluation of amorphous silica production from rice husk ashes. *Cleaner Production Journal*, 192, 688–697(2018), doi: 10.1016/j.jclepro.2018.05.028.

[20] D. Matei, D. L. Cursaru, and S. Mihai, Preparation of MCM-48 mesoporous molecular sieve influence of preparation conditions on the structural properties. *Digest Journal of Nanomaterials and Biostructures*, 1 (1). 271–276 (2016).

[21] D. Guliani, A. Sobti, and A. Pal, Comparative study on Graphene Oxide and MCM-48 based catalysts for esterification reaction. *Materials Today: Proceedings*, 41, 805–811 (2020), doi: 10.1016/j.matpr.2020.08.751.

[22] M. Wysocka-zolopa, I. Zablocka, A. Basa, and K. Winkler, Formation and characterization of mesoporous silica MCM-48 and polypyrrole composite. *Chemistry of Heterocyclic Compounds Journal*, 53 (1), 78–86 (2017), doi: 10.1007/s10593-017-2024-x.

[23] Y. Zeng, Fundamental Study of Adsorption and Desorption Process in Porous Materials with Functional Groups, *University of Queensland*, (2016).

[24] E. A. Ustinov, Nitrogen Adsorption on Silica Surfaces of Nonporous and Mesoporous Materials. *Langmuir Journal*, 24 (12), 6668–6675 (2008).

[25] C. T. Chiou, Fundamentals of the Adsorption Theory, *Partition and Adsorption of Organic Contaminants in Environmental Systems*, 39-52 (2002).

[26] F. Ambroz, T. J. Macdonald, V. Martis, and I. P. Parkin, Evaluation of the BET Theory for the Characterization of Meso and Microporous MOFs. *Small Methods Journal*, 2 (11), 1–17 (2018), doi: 10.1002/smtd.201800173.

[27] M. A. Al-ghouti and D. A. Da, Guidelines for the use and interpretation of adsorption isotherm models: A review. *Hazardous Materials Journal*, 393 (122383), (2020), doi: 10.1016/j.jhazmat.2020.122383.

[28] K. Sing, The use of nitrogen adsorption for the characterisation of porous materials. *Colloids and Surfaces Journal*, 188, 3–9 (2001).

[29] T. Salehi and D. Y. Kebria, Synergy of Granular Activated Carbon and Anaerobic Mixed Culture in Phenol Bioremediation of Aqueous Solution. *Iranian Journal of Energy and Environment*, 11 (3), 178–185 (2020), doi: 10.5829/ijee.2020.11.03.01.

[30] P. M. V Raja and A. R. Barron, Physical Methods in Chemistry and Nano Science. *Midas Green Innovation*, (2020).

[31] I. Langmuir, The Constitution and Fundamental Properties of Solids and Liquids. Part I. Solids. *American Chemical Society Journal*, 38 (11), 2221–2295 (1916), doi: 10.1021/ja02268a002.

[32] N. Ayawei, A. N. Ebelegi, and D. Wankasi, Modelling and Interpretation of Adsorption Isotherms, *Chemistry Journal*, (2017), doi: 10.1155/2017/3039817.

[33] M. A. I. Hourieh, M. N. Alaya, and A. M. Youssef, Analysis of Nitrogen Sorption Data of Chemically Activated Carbon by the Application of Adsorption Models Based on Surface Coverage

and Volume Filling of Micropores. *Adsorption Science & Technology Journal*, 17 (8), 675–688, (1999), doi: 10.1177/026361749901700806.

[34] H. M. F. Freundlich, over the adsorption in solution. *Physical Chemistry Journal*, 57 (38547157), 1100–1107 (1906).

[35] R. Saadi, Z. Saadi, R. Fazaeli, and N. E. Fard, "Monolayer and multilayer adsorption isotherm models for sorption from aqueous media. *Korean Journal of. Chemical Engineering*, 32 (5), 787–799 (2015), doi: 10.1007/s11814-015-0053-7.

[36] F. A. M.Belhachemi, Comparative adsorption isotherms and modeling of methylene blue onto activated carbons. *Applied Water Science Journal,* 1, 111–117 (2011), doi:10.1007/s13201-011-0014-1.

[37] P. Sinha, A. Datar, C. Jeong, X. Deng, Y. G. Chung, and L. Lin, Surface Area Determination of Porous Materials Using the Brunauer- Emmett-Teller (BET) Method: Limitations and Improvements. *Physical Chemistry Journal*, 123 (33), 20195-20209 (2019), doi: 10.1021/acs.jpcc.9b02116.

[38] V. S. Achari, A. S. Rajalakshmi, S. Jayasree, and R. M. Lopez, Surface Area and Porosity Development on Granular Activated Carbon by Zirconium: Adsorption Isotherm Studies. *Applied Research and Technology Journal*, 16, 211–228 (2018), doi: 10.22201/icat.16656423.0.16.3.719.

[39] F. J. V. A.Marcilla, A.G.Siurana, M.Munoz, Comments on the Methods of Characterization of Textural Properties of Solids from Gas Adsorption Data. *Adsorption Science & Technology Journal*, 27, 69–84 (2009).

[40] B. X. Medina-rodriguez and V. Alvarado, Use of Gas Adsorption and Inversion Methods for Shale Pore Structure Characterization. *Energies*, 14 (288014), (2021), doi:10.3390/en14102880.

[41] E. P. Barrett, L. G. Joyner, and P. P. Halenda, The Determination of Pore Volume and Area Distributions in Porous Substances. I. Computations from Nitrogen Isotherms. *American Chemical Society Journal*, 37 (13), 373–380, (1951), doi: 10.1021/JA01145A126.

[42] J. Choma, M. Jaroniec, and M. T. Academy, Improved Pore-size Analysis of Carbonaceous *Adsorbents. Adsorption Science & Technology Journal*, 20, 307–315 (2002), doi: 10.1260/026361702760254487.

[43] D. Dollimore and G. R. Heal, Pore-size distribution in typical adsorbent systems. *Colloid and Interface Science Journal*, 33 (4), 508–519 (1970), doi: 10.1016/0021-9797(70)90002-0.

[44] S. Geraedts, Pore size distribution and surface group analysis a study of two electrical grade carbon blacks. *Eindhoven University of Technology*, (2002).

[45] M. Thommes, K. Kaneko, A. V. Neimark, J. P. Olivier, F. R. Reinoso, J. Rouquerol and K. S. W. Sing, Physisorption of gases, with special reference to the evaluation of surface area and pore size distribution (IUPAC Technical Report*). Pure and Applied Chemistry Journal*, 87 (9), 1051–1069 (2015), doi: 10.1515/pac-2014-1117.

[46] C. Schlumberger and M. Thommes, Characterization of Hierarchically Ordered Porous Materials by Physisorption and Mercury Porosimetry — A Tutorial Review. *Advanced Materials Interfaces Journal*, 8, (2021), doi: 10.1002/admi.202002181.

[47] F. Adam, S. Balakrishnan, and P. Wong, Rice husk ash as a support material for thenium based heterogenous catalyst. *Physical Science Journal*, 17 (2), 1–13 (2006).

[48] K. Schumacher, P. I. Ravikovitch, A. D. Chesne, A. V. Neimark, and K. K. Unger, Characterization of MCM-48 Materials. *Langmuir Journal*, 16 (10), 4648–4654 (2000).

[49] A. Carati, G. Ferraris, M. Guidotti, G. Moretti, R. Psaro, and C. Rizzo, Preparation and characterisation of mesoporous silica-alumina and silicatitania with a narrow pore size distribution. *Catalysis Today Journal*, 77 (4), 315–323 (2003), doi: 10.1016/S0920-5861(02)00376-0.

[50] B. Coasne, A. Galarneau, F. D. Renzo, and R. J. M. Pellenq, Gas Adsorption in Mesoporous Micelle-Templated Silicas: MCM-41. *Langmuir Journal*, 22 (14), 11097–11105 (2006).

[51] A. Iqbal, N. A. M. Shuib, D. S. Darnis, M. Miskam, N. R. A. Rahman and F. Adam, Synthesis and Characterisation of Rice Husk Ash Silica Drug Carrier for α-Mangostin. *Physical Science Journal*, 29 (3), 95–107 (2018).